



CHORUS

This is the accepted manuscript made available via CHORUS. The article has been published as:

Magnetic field induced evolution of intertwined orders in the Kitaev magnet $\beta\text{-Li}_{2}\text{IrO}_{3}$

Ioannis Rousochatzakis and Natalia B. Perkins

Phys. Rev. B **97**, 174423 — Published 24 May 2018

DOI: [10.1103/PhysRevB.97.174423](https://doi.org/10.1103/PhysRevB.97.174423)

Magnetic field-induced evolution of intertwined orders in the Kitaev magnet $\beta\text{-Li}_2\text{IrO}_3$

Ioannis Rousochatzakis and Natalia B. Perkins

School of Physics and Astronomy, University of Minnesota, Minneapolis, MN 55116, USA

Recent scattering experiments in the 3D Kitaev magnet $\beta\text{-Li}_2\text{IrO}_3$ have shown that a relatively weak magnetic field along the crystallographic **b**-axis drives the system from its incommensurate counter-rotating order to a correlated magnet, with a significant uniform ‘zigzag’ component superimposing the magnetization along the field. Here it is shown that the zigzag order is not emerging from its linear coupling to the field (via a staggered, off-diagonal element of the **g**-tensor), but from its intertwining with the incommensurate order and the longitudinal magnetization. The emerging picture explains all qualitative experimental findings at zero and finite fields, including the rapid decline of the incommensurate order with field and the so-called intensity sum rule. The latter are shown to be independent signatures of the smallness of the Heisenberg exchange J , compared to the Kitaev coupling K and the off-diagonal anisotropy Γ . Remarkably, in the regime of interest, the field H^* at which the incommensurate component vanishes, depends essentially only on J , which allows to extract an estimate of $J \simeq 4$ Kelvin from reported measurements of H^* . We also comment on recent experiments in pressurized $\beta\text{-Li}_2\text{IrO}_3$ and conclude that J decreases with pressure.

I. Introduction

The realization^{1,2} that certain correlated materials based on 4d and 5d transition metals, like Ir^{4+} or Ru^{3+} , host the key microscopic ingredients for the so-called Kitaev spin liquid³ has spurred tremendous experimental and theoretical interest in the last decade^{4–9}. A recurring theme in this research is that the predicted quantum spin liquids^{3,10–12} are fragile against various realistic perturbations^{2,13–19} and are preempted by magnetic order at low enough temperatures^{20–29}. Nevertheless, there is overwhelming evidence that external perturbations, such as magnetic field^{30–42}, chemical substitution^{43,44}, or pressure^{29,37,45–52}, can drive these materials to various types of correlated phases, including spin liquids. To go forward, it is therefore crucial to map out the most relevant instabilities, and identify their distinctive experimental fingerprints.

In this vein, we study the enigmatic magnetic-field induced instability reported recently by Ruiz *et al*³⁶ in the 3D hyperhoneycomb iridate $\beta\text{-Li}_2\text{IrO}_3$ ^{28,29}. At zero field, this magnet was known²⁸ to develop (below $T_N = 37$ Kelvin) a counter-rotating incommensurate (IC) modulation, similar with those in the 3D stripy-honeycomb $\gamma\text{-Li}_2\text{IrO}_3$ ^{26,27} and the layered honeycomb $\alpha\text{-Li}_2\text{IrO}_3$ ²⁵. The new findings from the magnetic resonant X-ray scattering data under a finite field are the following³⁶: (i) The IC order of $\beta\text{-Li}_2\text{IrO}_3$ is very fragile against a magnetic field along the crystallographic **b**-axis, and disappears completely at a characteristic field H^* . (ii) The system develops a significant uniform ‘zigzag’ component along **a** (superimposing the magnetization along **b**), similar to the zigzag order of Na_2IrO_3 ^{20–22,53–55} and $\alpha\text{-RuCl}_3$ ^{23,24,56–59}. (iii) The zigzag component grows linearly with field until it shows a kink at H^* , but is otherwise undetectable at zero field, consistent with the experiments of Biffin *et al*²⁸. (iv) Quite surprisingly, the sum of the intensities of the Bragg peaks associated with the IC and the uniform components (rescaled by some factor) remains constant up to a field slightly larger than H^* .

One way to rationalize the appearance of the zigzag component is to build on the insight that a field along **b** couples linearly not only to the uniform magnetization along **b**, but also to the zigzag component along **a**, by virtue of the off-

diagonal element g_{ab} of the **g**-tensor.³⁶ This would explain the growth of the zigzag component (besides the magnetization along **b**) at the expense of the IC order. However, this picture of a field-induced zigzag order cannot readily explain the significant zigzag amplitude at H^* , the intensity sum rule (point (iv) above), as well as the T -dependence of the intensity of the zigzag component, which is very similar to that of an order parameter³⁶.

The results presented below reveal that a more consistent scenario is that the IC counter-rotating component, the zigzag component along **a** and the magnetization along **b** are intertwined components of the same order. It is shown in particular, that the significant growth of the zigzag component with field occurs even in the absence of the off-diagonal element g_{ab} . This demonstrates that the zigzag component does not originate in its linear coupling to the field, but rather in an intrinsic coupling with the IC order and the magnetization along **b**. In fact, as shown in Ref. [60], both the zigzag component and the magnetization along **b** are already present at zero field, albeit with an amplitude that is too weak to be detected.

The emerging picture explains all the qualitative experimental results at both zero²⁸ and finite fields³⁶. First, the weak zigzag amplitude at zero-field, the rapid decline of the IC order with field, and the intensity sum rule are all facets of the same fact. Namely, that the Heisenberg coupling J is much weaker than both the Kitaev interaction K and the off-diagonal exchange anisotropy Γ . Second, the characteristic field H^* is essentially independent of the dominant interactions K and Γ and scales linearly with J . This allows to deduce an estimate of $J \simeq 4$ Kelvin from reported data of H^* . Furthermore, a comparison with recent experiments under pressure³⁷ suggests that J decreases (below 4 Kelvin) with pressure.

The present work builds on the recent study by Ducatman *et al*⁶⁰, which is based on the intuitive idea that the observed IC order²⁸ can be thought of as a long-wavelength twisting of a nearby commensurate order, called the ‘ K -state’ [see Fig. 1 (a)], with the same qualitative features. Namely, the same propagation vector (with periodicity very close to the experimental value 0.57), the same irreducible representation, the counter-rotating moments, and non-coplanarity. The

present study essentially addresses the fate of this K -state under a field along the \mathbf{b} -axis. But first, let us repeat the most important aspects of the system and the zero-field K -state.⁶⁰

II. Lattice structure and microscopic spin model

The lattice structure of β -Li₂IrO₃ has been discussed in detail elsewhere.^{28,36,60–62} The Ir ions form interwoven networks of two types of ‘zig-zag’ chains, one propagating along $\hat{\mathbf{a}}+\hat{\mathbf{b}}$ and the other along $\hat{\mathbf{a}}-\hat{\mathbf{b}}$. The first type of chains comprise the nearest-neighbor (NN) bonds denoted by x and y in Fig. 1 (b), while the second type comprise the NN bonds denoted by x' and y' . We shall refer to these as xy - and $x'y'$ -chains, respectively. Finally, the two chain types are connected via NN bonds that are oriented along the $\hat{\mathbf{c}}$ -axis and are denoted by z in Fig. 1 (b).

The microscopic J - K - Γ model, introduced by Lee *et al.*,^{61,62} features three types of NN interactions, the Heisenberg exchange J , the Kitaev anisotropy K and the off-diagonal symmetric anisotropy Γ . For a given bond of type t , between NN sites i and j , the total interaction takes the form

$$\mathcal{H}_{ij}^{(t)} = JS_i \cdot S_j + KS_i^{\alpha_t} S_j^{\alpha_t} + \sigma_t \Gamma (S_i^{\beta_t} S_j^{\gamma_t} + S_i^{\gamma_t} S_j^{\beta_t}), \quad (1)$$

where $(\alpha_t, \beta_t, \gamma_t) = (x, y, z)$ for $t \in \{x, x'\}$, (y, z, x) for $t \in \{y, y'\}$, and (z, x, y) for $t = z$. The prefactor σ_t of the Γ terms is $+1$ for $t \in \{x, z, y'\}$ and -1 for $t \in \{y, x'\}$. This modulation of the prefactors is tied to the following convention for the relation between the crystallographic axes $\{\hat{\mathbf{a}}, \hat{\mathbf{b}}, \hat{\mathbf{c}}\}$ and the Cartesian axes $\{\hat{\mathbf{x}}, \hat{\mathbf{y}}, \hat{\mathbf{z}}\}$ ⁶³:

$$\hat{\mathbf{x}} = \frac{\hat{\mathbf{a}}+\hat{\mathbf{c}}}{\sqrt{2}}, \quad \hat{\mathbf{y}} = \frac{\hat{\mathbf{c}}-\hat{\mathbf{a}}}{\sqrt{2}}, \quad \hat{\mathbf{z}} = -\hat{\mathbf{b}}. \quad (2)$$

The total Hamiltonian in a field \mathbf{H} takes the form

$$\mathcal{H} = \sum_t \sum_{\langle ij \rangle \in t} \mathcal{H}_{ij}^{(t)} - \mu_B \mathbf{H} \cdot \sum_i \mathbf{g}_i \cdot \mathbf{S}_i, \quad (3)$$

where μ_B is the Bohr magneton and \mathbf{g}_i is the electronic \mathbf{g} -tensor at site i . In the following, we work in units of $\sqrt{J^2 + K^2 + \Gamma^2} = 1$ and use the parametrization^{60–62}:

$$J = \sin r \cos \phi, \quad K = \sin r \sin \phi, \quad \Gamma = -\cos r, \quad (4)$$

where $\phi \in [0, 2\pi)$, $r \in [0, \pi/2]$. In particular, we shall focus on the ‘ K -region’ of Fig. 1 (a). As argued in Ref.⁶⁰, the actual IC order inside this region can be thought of as a long-wavelength twisting of a nearby commensurate state, called the ‘ K -state’. This state is a local minimum of the energy, except at $\phi = 3\pi/2$ where it is one of the global minima (which form an S^2 manifold), and probably survives as such in a small finite window of ϕ above $3\pi/2$ due to the lattice cutoff.⁶⁰ Nevertheless, this state has all qualitative features of the experimentally observed IC order at zero field⁶⁰.

III. Main aspects of the zero-field K -state

The detailed structure of the K -state is discussed in Ref.⁶⁰. A schematic representation is shown in Fig. 1 (b). Let us repeat here the main features that are needed for our pur-

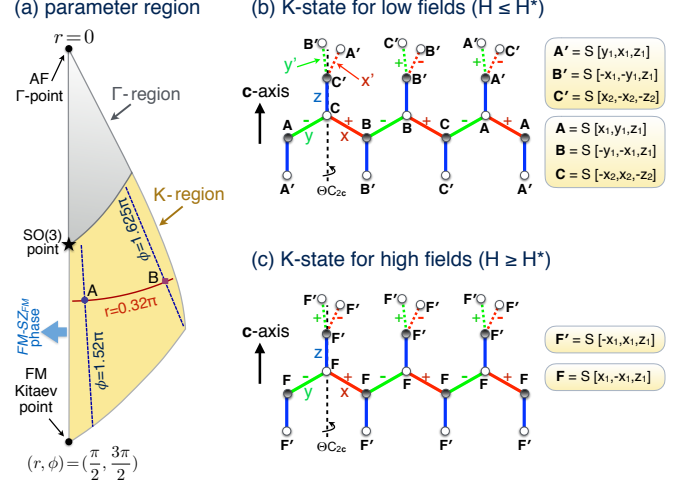


FIG. 1. (a) The relevant parameter space in (r, ϕ) [see Eq. (4)], along with the K - and Γ -regions proposed in Ref. [60]. The points A and B , referred to in subsequent figures, correspond to $(r, \phi) = (0.32\pi, 1.52\pi)$ and $(0.32\pi, 1.625\pi)$. (b-c) The structure of the K -state at low ($H \leq H^*$) and high ($H \geq H^*$) fields. The solid (dashed) green and red bonds depict the xy ($x'y'$) chains running along $\hat{\mathbf{a}}+\hat{\mathbf{b}}$ ($\hat{\mathbf{a}}-\hat{\mathbf{b}}$). The blue vertical segments point along the \mathbf{c} -axis and depict the z -bonds. The Cartesian components of the spins are shown in the side panels. Both states respect the combined operation ΘC_{2c} , where Θ is time reversal and C_{2c} is the two-fold rotation around \mathbf{c} . The high-field K -state is qualitatively similar to the state ‘FM-SZFM’ of Ref. [61], which is stabilized in a finite region with $\phi < 3\pi/2$.

poses. The K -state features six spin sublattices, three (\mathbf{A} , \mathbf{B} , \mathbf{C}) along the xy -chains and three (\mathbf{A}' , \mathbf{B}' , \mathbf{C}') along the $x'y'$ -chains. The corresponding Cartesian components are given in the side panels of Fig. 1 (b), where $S = 1/2$ is the classical spin length, while the numbers x_1, y_1, z_1, x_2 and z_2 are all positive (at zero field), and obey the constraints $x_1^2 + y_1^2 + z_1^2 = 1$ and $2x_2^2 + z_2^2 = 1$.

The sublattices $\{\mathbf{A}, \mathbf{B}, \mathbf{C}\}$ (and likewise the sublattices $\{\mathbf{A}', \mathbf{B}', \mathbf{C}'\}$) form an almost ideal 120° -pattern. The counter-rotating modulation of the moments can be seen in Fig. 1 (b) by noticing that, along the xy -chains (similarly for the $x'y'$ -chains), the odd sites (gray circles) modulate in a $\mathbf{ABCAB}\dots$ pattern, while the even sites (white circles) show a $\mathbf{CBACB}\dots$ pattern. This modulation shows up in the Fourier component of the static structure factor at $\mathbf{Q} = 2\hat{\mathbf{a}}/3$, which takes the characteristic form $\mathbf{M}_{\mathbf{Q}=2\hat{\mathbf{a}}/3} = (iM_a A, iM_b C, M_c F)$, along \mathbf{a} , \mathbf{b} and \mathbf{c} . Here, A , C and F denote, respectively, the Néel, stripy and FM basis vectors of the 4-site unit cell^{28,60}. The amplitudes M_a , M_b and M_c are given by⁶⁰

$$M_a = i2S(x_1 + 2x_2 - y_1), \quad M_b = -i2S(z_1 + z_2), \quad M_c = i2S\sqrt{3}(x_1 + y_1). \quad (5)$$

The counter-rotating modulation is however not the only component of the K -state, because there are two types of deviations from the ideal 120° -pattern when $\phi > 3\pi/2$: i) an in-plane canting of the zigzag type, whose direction alternates

between \mathbf{a} and $-\mathbf{a}$ for xy - and $x'y'$ -chains, respectively, and ii) an out-of-plane ferromagnetic (FM) canting along \mathbf{b} . Both of these cantings are uniform from one unit cell to another, and show up directly in the $\mathbf{Q} = 0$ Fourier component of the static spin structure factor, along \mathbf{a} and \mathbf{b} . Specifically, $\mathbf{M}_{\mathbf{Q}=0} = (M'_a G, M'_b F, 0)$, where G and F denote, respectively, the zigzag and FM basis vectors of the 4-site primitive unit cell^{28,60}. The amplitudes M'_a and M'_b are⁶⁴

$$M'_a = -4S(x_1 - y_1 - x_2), \quad M'_b = 2S(2z_1 - z_2). \quad (6)$$

These amplitudes vanish when $J \rightarrow 0^+$, because in this limit $\{\mathbf{A}, \mathbf{B}, \mathbf{C}\}$ and $\{\mathbf{A}', \mathbf{B}', \mathbf{C}'\}$ reach their ideal 120° -patterns.

IV. Total Energy of the K -state in a field

We now move to the main part of this study and analyze the fate of the K -state under a field H along the \mathbf{b} -axis. As discussed in detail in Ref.³⁶, the total polarization along \mathbf{b} couples to the field via the diagonal element g_{bb} of the \mathbf{g} -tensor, while the uniform zigzag canting along \mathbf{a} (i.e., the staggered magnetization from xy - to $x'y'$ -chains), couples to the field via the off-diagonal element g_{ab} , whose sign alternates between xy and $x'y'$ chains due to the two-fold symmetry C_{2a} that passes through the middle of the z bonds. So, a magnetic field along \mathbf{b} couples linearly to both M'_a and M'_b . Furthermore, such a field does not break the symmetry ΘC_{2c} obeyed by the K -state, see Fig. 1 (b). These arguments suggest that we can use the K -state ansatz [side panel of Fig. 1 (b)], but now the coefficients x_1, y_1 , etc will change with the field. To find these coefficients we must minimize the total energy,

$$\begin{aligned} E/N = S^2 \left\{ K [3 - 2(y_1 - x_2)^2] \right. \\ + 2\Gamma [1 - z_1^2 + x_2^2 + 2(y_1 + x_2)z_1 + 2x_1z_2] \\ + J [1 + 2(z_1 - z_2)^2 - 4x_1x_2 + 4(x_1 + x_2)y_1] \left. \right\} / 6 \\ - \mu_B H S [\sqrt{2}g_{ab}(x_1 - x_2 - y_1) + g_{bb}(-2z_1 + z_2)] / 3, \end{aligned} \quad (7)$$

(N is the total number of sites) for given H, J, K, Γ, g_{bb} , and g_{ab} . From x_1, y_1 , etc we can then deduce the various components of the structure factor using Eqs. (5) and (6).

The anisotropy of the local \mathbf{g} -tensors is set by the local environment of the iridium-oxygen octahedra, and in particular the trigonal distortion and the rotation of the octahedra. However, both of these are very small in β - Li_2IrO_3 , see e.g., Fig. 1(b) in Ref. [29] and Supplemental Material of Ref. [36]. So, in the following we shall take $g_{bb} = 2$ and $g_{ab} = \pm 0.1$. We will in fact show in Sec. VII that the evolution of the magnetization is almost the same with that for $g_{ab} = 0$.

V. Main results

Let us first highlight the results that are directly related to the reported experiments. For demonstration, we have taken $g_{bb} = 2$ and $g_{ab} = 0.1$ (we shall address the role of g_{ab} separately below). Figs. 2 (a) and (b) show the magnitudes of the various Fourier components, at the points A and B of Fig. 1 (a). The results show that the $\mathbf{Q} = 2\hat{\mathbf{a}}/3$ components, M_a, M_b and M_c , decline with the field, and vanish completely

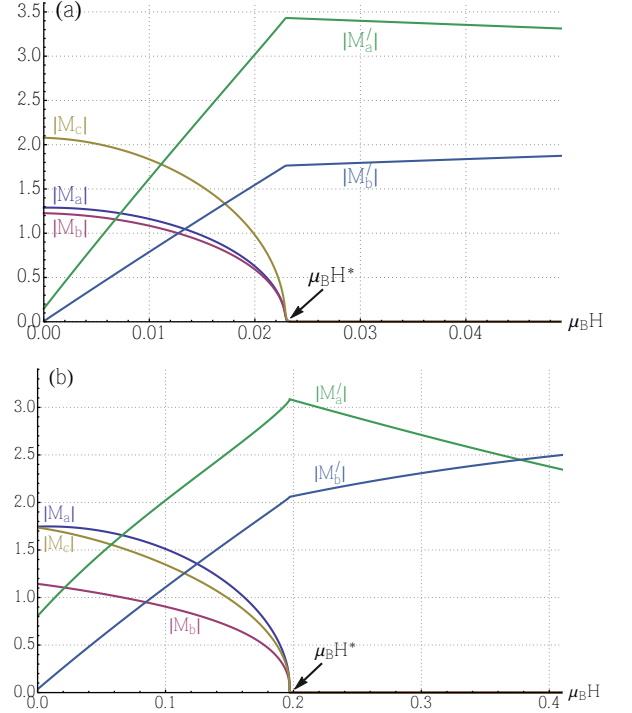


FIG. 2. Evolution of the various Fourier components of the static structure factor of the K -state with a magnetic field H along \mathbf{b} , for the points A (panel a) and B (panel b) in Fig. 1 (a).

at (and above) a characteristic field H^* . At the same time, the $\mathbf{Q} = 0$ components, M'_a and M'_b , grow linearly with the field, and they show a kink at H^* . These results are consistent with the data reported in Ref. [36].

We can also see an important feature of the $\mathbf{Q} = 0$ components, which is related to the zero-field scattering experiments of Biffin *et al.*²⁸. Namely, that both $|M'_a(0)|$ and $|M'_b(0)|$ are very small when ϕ is close to $3\pi/2$ [see Fig. 2 (a)], where both the zigzag and the FM canting become small. As we move away from the line $\phi = 3\pi/2$, the zigzag amplitude $M'_a(0)$, in particular, is not small any longer, see Fig. 2 (b). So, the absence of the $\mathbf{Q} = 0$ Bragg peaks from the zero-field scattering experiments of Biffin *et al.*²⁸ is the first evidence that ϕ is close to $3\pi/2$, i.e., that J is much weaker than both K and Γ .

The next qualitative experimental result that we would like to address is the intensity sum rule of Ref. [36], i.e. the finding that the sum of a certain combination of the intensities corresponding to zero- and finite- Q Bragg peaks, remains almost constant even slightly above H^* . To this end, we will need to understand the behavior of the coefficients x_1, y_1 , etc first.

From Eqs. (5-6) we find that the simultaneous vanishing of M_a, M_b and M_c for $H \geq H^*$ imply that

$$H \geq H^* : x_1 = -y_1 = -x_2, \quad z_2 = -z_1. \quad (8)$$

These relations are indeed satisfied as we see in Fig. 3. In particular, while all coefficients are positive at zero field, the coefficients y_1, x_2 and z_1 change sign at some intermediate field, and eventually satisfy (8) for $H \geq H^*$.

The explanation of the intensity sum rule reported in

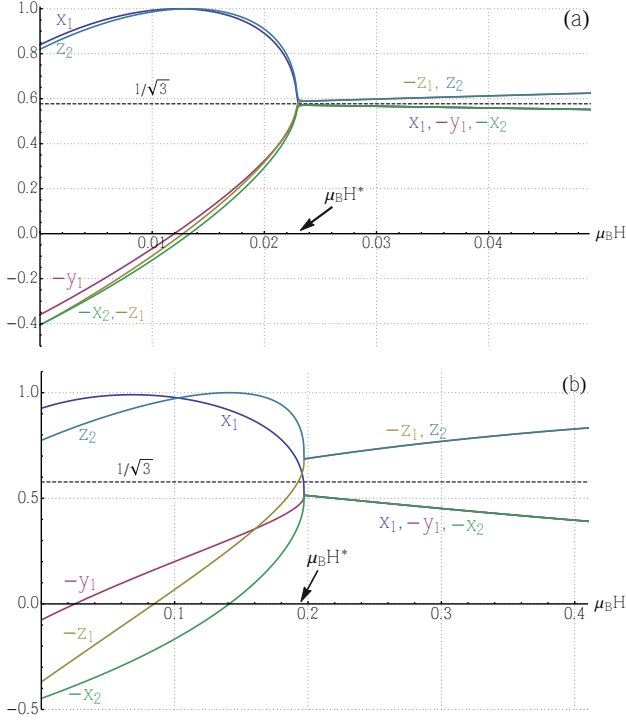


FIG. 3. Evolution of the coefficients x_1 , y_1 , etc with a magnet field H along \mathbf{b} , for the points A (panel a) and B (panel b) in Fig. 1 (a)

Ref. [36] stems from another aspect of Fig. 3 (a), namely, that

$$H \leq H^*, \quad \phi \rightarrow \left(\frac{3\pi}{2}\right)^+ : \begin{cases} z_2 \simeq x_1, & x_2 \simeq z_1 \simeq y_1, \\ x_1(0) \simeq \sqrt{2/3}, & y_1(0) \simeq 1/\sqrt{6}. \end{cases} \quad (9)$$

Remarkably, these approximate relations hold all the way down to zero field, where they stem from the special structure of the ground state manifold along $\phi = 3\pi/2$, and the concomitant lifting of the degeneracy by an infinitesimal positive J .⁶⁰ For larger J , the approximations in Eq. (9) become progressively worse as shown in Fig. 3 (b).

Now, to see how Eq. (9) leads to the intensity sum rule, we take the following combinations of the Bragg peak intensities,

$$I_I = |M_a|^2 + |M_b|^2 + |M_c|^2, \quad I_V = |M'_a|^2 + |M'_b|^2. \quad (10)$$

Fig. 4 shows the behavior of the quantities $I_I/I_I(0)$, $\alpha I_V/I_I(0)$ and $I_{\text{tot}} \equiv (I_I + \alpha I_V)/I_I(0)$, where the constant $\alpha \equiv I_I(0)/I_V(H^*)$ fixes $I_{\text{tot}}(H^*) = 1$. We first discuss the results shown in Fig. 4 (a), which are obtained at the point A of Fig. 1 (a). As expected, the intensity associated with the counter-rotating component of the order, I_I , declines quickly with field, while the intensity associated with the uniform components, I_V , grows quadratically with field up to H^* . At the same time, the total intensity I_{tot} remains extremely close to 1 from zero field all the way up to H^* . This behavior is fully consistent with the intensity sum rule of Fig. 4 (a) of Ref. [36].

Importantly, while it is not clear which exact combinations of the zero- and finite- Q intensities are involved in the sum rule reported in Ref. [36], we can show that this does not mat-

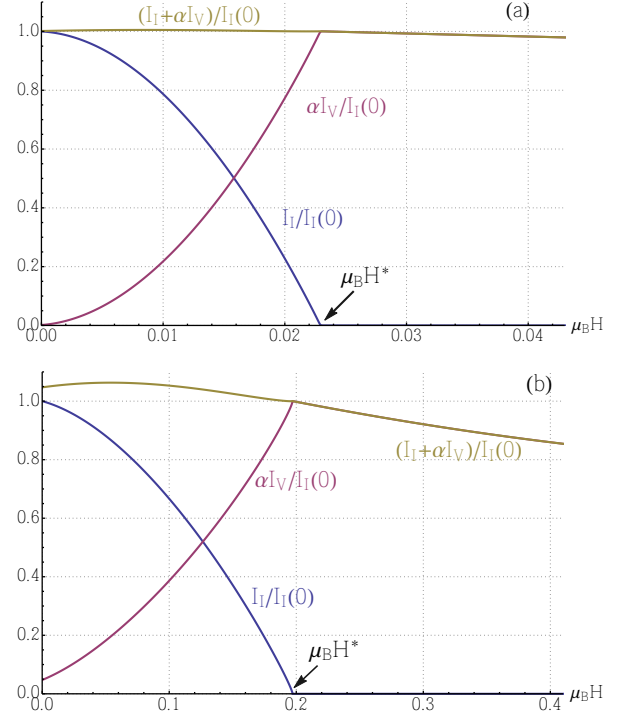


FIG. 4. Evolution of the combinations I_I , I_V and I_{tot} [see Eq. (10)] with a magnetic field H along \mathbf{b} , for the points A (panel a) and B (panel b) of Fig. 1 (a). In (a), $\alpha \simeq 0.503$ [very close to the expected value of $1/2$ when $\phi \rightarrow (3\pi/2)^+$, see text], while in (b), $\alpha \simeq 0.535$.

ter as long as we are close to the line $\phi = 3\pi/2$, where the approximate relations (9) hold. Indeed, these relations give:

$$H \leq H^*, \quad \phi \rightarrow \left(\frac{3\pi}{2}\right)^+ : \begin{cases} |M_a|^2 \simeq |M_b|^2 \simeq \frac{1}{3}|M_c|^2 \simeq (x_1 + y_1)^2, \\ |M'_b|^2 \simeq \frac{1}{4}|M'_a|^2 \simeq (x_1 - 2y_1)^2. \end{cases} \quad (11)$$

This implies that any linear combination among $\{|M_a|^2, |M_b|^2, |M_c|^2, |M'_a|^2, |M'_b|^2\}$ will always be of the form $(x_1 + y_1)^2 + \beta(x_1 - 2y_1)^2$, which, in turn, becomes independent of H if we choose $\beta = 1/2$ (using the spin length constraint $1 = x_1^2 + y_1^2 + z_1^2 \simeq x_1^2 + 2y_1^2$). This value is consistent with the limiting value of α defined above when $\phi \rightarrow (3\pi/2)^+$.

The intensity sum rule is no longer satisfied as we go further away from $\phi = 3\pi/2$. This can be seen in Fig. 4 (b), which shows I_I , I_V and I_{tot} computed at the point B of Fig. 1 (a). The total intensity I_{tot} deviates from the value 1 in the entire region between $H = 0$ and $H = H^*$, except at H^* where it is fixed to 1 by definition. We also see that I_{tot} shows a fast drop below 1 at $H > H^*$, in contrast to the experimental data,³⁶ but also in contrast to the data of Fig. 4 (a), where the corresponding drop at $H > H^*$ is much slower. Note also that the overall deviation from the sum rule could be even worse for linear combinations of $\{|M_a|^2, |M_b|^2, |M_c|^2, |M'_a|^2, |M'_b|^2\}$ other than the ones involved in I_I and I_V . We can therefore safely conclude that the experimental observation of the sum rule is an independent signature of the smallness of J .

VI. Nature of the high-field state ($H \geq H^*$)

Based on Eq. (8), the Cartesian components of the various spin sublattices for $H \geq H^*$ are:

$$H \geq H^* : \begin{cases} \mathbf{A} = \mathbf{B} = \mathbf{C} = S[x_1, -x_1, z_1], \\ \mathbf{A}' = \mathbf{B}' = \mathbf{C}' = S[-x_1, x_1, z_1], \end{cases} \quad (12)$$

see Fig. 1 (c). So the xy - and $x'y'$ -chains form two separate FM subsystems, which give a total FM moment along $-\mathbf{z} = \mathbf{b}$ [$z_1(H^*)$ is negative] and a staggered, zigzag moment along $\frac{x-y}{\sqrt{2}} = \mathbf{a}$ [see Eq. (2)]. This state is qualitatively the same with the state 'FM-SZ_{FM}' reported by Lee *et al*^{61,62} for $\phi < 3\pi/2$, see Fig. 1 (a). The only difference is that in that state $x_1 = \frac{1}{\sqrt{3}}$, while here x_1 in general deviates from this value and depends on the field. However, x_1 becomes very close to $\frac{1}{\sqrt{3}}$ precisely at $H = H^*$ when $\phi \rightarrow (3\pi/2)^+$, see Fig. 3 (a). So, the effect of the field is to suppress the counter-rotating component of the state and, at the same time, effectively drive the system towards the state that is stabilized for negative J . Intuitively then, the field plays the role of a FM Heisenberg coupling that counteracts the effect of J (which is positive). This also tells us that the field H^* required to achieve this must be proportional to J , and we will confirm this below.

Now, the approximate relation $x_1(H^*) \approx \frac{1}{\sqrt{3}}$ for $\phi \rightarrow (2\pi/3)^+$ gives, based on Eq. (6), $M'_a(H^*) \approx -2\sqrt{3}$ and $M'_b(H^*) \approx -\sqrt{3}$, see Fig. 2 (a). Remarkably, these values are independent of the ratio K/Γ , as long as we are inside the K -region of Fig. 1 (a) and close to the line $\phi = 3\pi/2$. Furthermore, imposing (8) to (7) and minimizing the resulting expression for E/N gives an implicit relation for $x_1(H)$:

$$H \geq H^* : \mu_B H = 2S \frac{\Gamma(4x_1^2 - 1) + (2J - \Gamma)x_1\sqrt{1 - 2x_1^2}}{2g_{bb}x_1 - \sqrt{2}g_{ab}\sqrt{1 - 2x_1^2}}. \quad (13)$$

Note that K does not appear explicitly in this relation, which can give the wrong impression that H^* does not depend on K . This is however not true, because H^* and $x_1(H^*)$ cannot be both determined solely by Eq. (13).

Eq. (13) gives the large-field behavior of M'_a and M'_b ,

$$H \geq H^* : M'_a = -12Sx_1, \quad M'_b = -6S\sqrt{1 - 2x_1^2}. \quad (14)$$

The large-field behavior of x_1 , $|M'_a|$ and $|M'_b|$ are shown in Figs. 7 and 8. In the infinite-field limit, in particular,

$$H \rightarrow \infty : M'_a \rightarrow -\frac{6g_{ab}}{\sqrt{2}\sqrt{g_{ab}^2 + g_{bb}^2}}, \quad M'_b \rightarrow -\frac{3g_{bb}}{\sqrt{g_{ab}^2 + g_{bb}^2}}. \quad (15)$$

With $g_{ab} \ll g_{bb}$ we get $M'_a \simeq 0$, $M'_b \simeq -3$, $x_1 \simeq 0$, $z_1 \simeq -1$, and $\mathbf{A} = \mathbf{B} = \mathbf{C} = \mathbf{A}' = \mathbf{B}' = \mathbf{C}' = S\mathbf{b}$, as expected.

VII. The role of g_{ab} and the origin of the zigzag component

As announced in the Introduction, the significant growth of the zigzag component under the field along \mathbf{b} does not originate in the linear coupling between the zigzag component and the field, via g_{ab} . This is shown in Fig. 5 where we compare

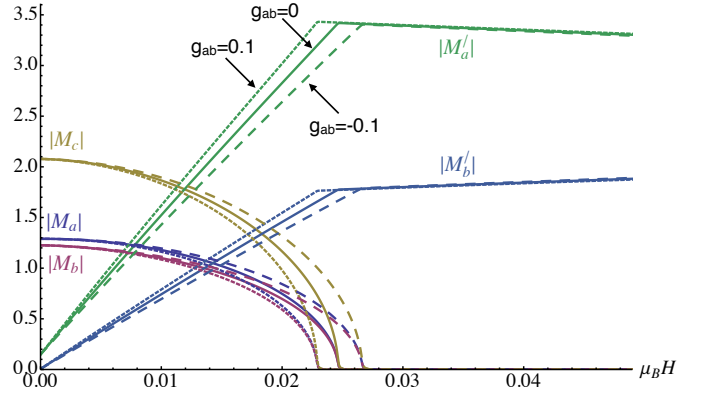


FIG. 5. Effect of g_{ab} on the evolution of the various components of the structure factor. Data are taken at the point A of Fig. 1 (a), with $g_{bb} = 2$ and $g_{ab} = 0.1$ [dotted lines, same as in Fig. 2 (a)], 0 (solid) and -0.1 (long-dashed).

the response shown already in Fig. 2 (a) for $g_{ab} = 0.1$, with the response for $g_{ab} = 0$ and $g_{ab} = -0.1$. The comparison of the various components of the structure factor computed at $g_{ab} = 0.1$ and $g_{ab} = 0$ shows that, while H^* shifts to slightly higher value for $g_{ab} = 0$, the large size of the zigzag component at H^* remains robust. A further comparison to the case of $g_{ab} = -0.1$ shows that even the choice of the sign of g_{ab} , which has been arbitrarily considered to be positive so far [i.e., positive (negative) on the xy ($x'y'$) bonds], does not alter the large magnitude of $|M'_a(H^*)|$. Taken together, these results show that, although M'_a couples linearly to the field via g_{ab} , its significant growth is not related to g_{ab} but to an inherent tendency of the system to reach the state described by Eq. (12). This state has already a finite component at zero-field, although its amplitude is undetectable for weak J .

VIII. Dependence of H^* on model parameters

We now turn to the important question of the dependence of the characteristic field H^* on the coupling parameters. To address this question we have calculated H^* for various paths in parameter space and the results are shown in Fig. 6. Panel (a) shows the evolution of H^* with K , for fixed $\Gamma = -1$ and various values of J , while panel (b) shows the evolution of H^* with Γ for fixed $K = -1$ and the same set of J values as in panel (a). The results from panels (a) and (b) can be summarized as follows. (i) H^* tends to decrease with increasing $|K|$ and $|\Gamma|$. (ii) The rate of this decrease is almost zero at small J and then increases with increasing J . (iii) H^* has a much stronger dependence on J compared to its dependence on K and Γ . In particular, H^* grows with increasing J , with an almost constant rate.

These features can also be seen in panel (c), which shows the data collected from (a) and (b), with J on the horizontal axis. This figure shows explicitly that for small enough J , H^* is essentially independent of K and Γ [point (ii) above] and grows linearly with J [point (iii) above]. It also shows that the deviation from this linear growth becomes larger for larger J , where a dependence on K and Γ shows up.

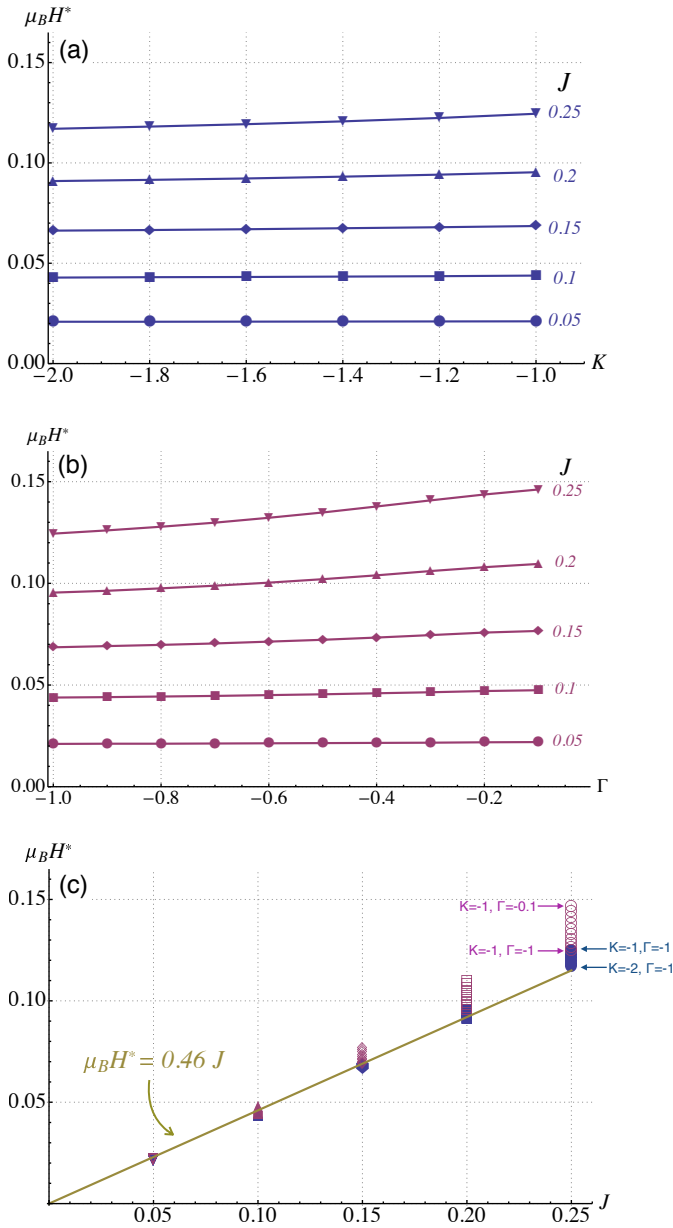


FIG. 6. (a) Evolution of H^* as a function of K for fixed $\Gamma = -1$ and various values of J . (b) Evolution of H^* as a function of Γ for fixed $K = -1$ and various values of J . (c) Collected data shown in panels (a) and (b), with J on the horizontal axis. The line shown in a guide to the eye. For all cases we have taken $g_{ab} = 0.1$ and $g_{bb} = 2$.

IX. Discussion

The results presented here provide a consistent interpretation of the recent scattering experiments by Ruiz *et al.*³⁶. First, the analysis confirms the linear growth of a uniform zigzag component along a, the rapid decline of the IC order, and the intensity sum rule. The latter two observations are signatures of the smallness of J compared to K and Γ .

Second, the significant growth of the zigzag component under the field does *not* stem from their linear coupling, as the zigzag amplitude at H^* remains almost the same in the absence of this coupling (i.e., for $g_{ab} = 0$). This shows a strong

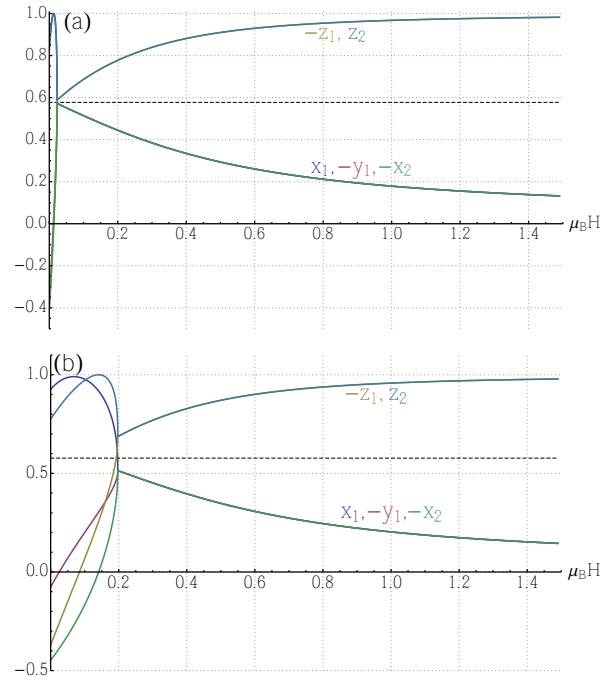


FIG. 7. Same as in Fig. 3 but now we show the behavior up to fields much higher than H^* . Panels (a) and (b) correspond again to the parameter points A and B, respectively, of Fig. 1 (a).

intertwining of the zigzag component to both the IC counterrotating component and the longitudinal magnetization, which is the one most directly driven by the field. Moreover, the zigzag component is already present at zero field (the same is true for the magnetization along b) but, for weak J , its amplitude is too weak to be observed, consistent with Ref. [28].

Third, the field acts effectively as a FM Heisenberg coupling that counteracts the effect of J , and the state reached at H^* is qualitatively the same as the state stabilized by a negative J at zero field. An immediate ramification is that H^* grows linearly with J , which is demonstrated numerically in the relevant regime of interest. Accordingly, the rapid decline of the IC component is another signature of the smallness of J . In particular, the curve shown in Fig. 6(c) gives $J \simeq 4$ Kelvin for the experimental value of $H^* = 2.8$ T³⁶ (assuming $g_{bb} = 2$ and $g_{ab} = 0.1$; the latter does not affect H^* as strongly as g_{bb}), which is indeed much smaller⁶⁵ than the reported *ab initio* values of K and Γ ^{37,49,66}.

Given this, the recent report³⁷ that H^* decreases with pressure is direct evidence (within the J - K - Γ framework) that J decreases under pressure. However, the behavior of H^* alone cannot tell us what happens to K and Γ , because H^* shows a weak dependence on these couplings only at larger J ; There is however independent evidence from μ SR³⁷ and *ab initio* calculations^{37,49} showing that pressure increases the ratio $|\Gamma/K|$, with the system approaching the correlated classical spin liquid regime of the large- Γ model⁶⁷.

An experimental result that is not readily captured by the present classical description is the reported value of the magnetization at H^* per Ir site, $m/\mu_B \simeq 0.31$ ³⁶, which is about

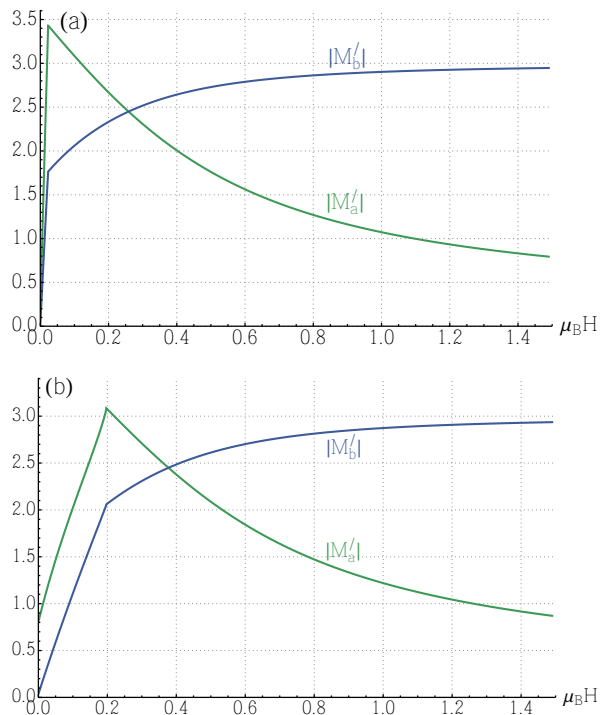


FIG. 8. Same as in Fig. 2 but now we show the behavior up to fields much higher than H^* . Panels (a) and (b) correspond again to the parameter points A and B , respectively, of Fig. 1 (a).

two times smaller than the value $z_1(H^*)g_{bb}S \simeq \frac{1}{\sqrt{3}}$ (for weak J and $g_{ab} = 2$), deduced from the above analysis. Given that the IC component disappears at H^* , the discommensurations that are missed by the K -state ansatz at zero field⁶⁰ are not present any longer. Therefore, the above large disagreement in the magnetic moment m should be attributed to the reduction of the spin length by quantum fluctuations. Such an unusually⁶⁸ large reduction can only be expected close to the frustrated region $\phi \sim 3\pi/2$, which is in line with the remaining evidence above. A standard $1/S$ expansion around the

K -state at H^* should confirm this picture, but this is out of the scope of the present study.

We should note here that while the actual system deviates from the symmetric, nearest-neighbor (NN), J - K - Γ model that we use here, the agreement with the reported experiments gives strong confidence that this minimal model provides an excellent starting point, and that additional perturbations are too weak to play a qualitative role. Physically, this is related to the stability of the ‘ K -state’ against these perturbations.

The broader emerging picture, taken together with the evidence from the zero-field study of Ref. [60], gives also confidence to the intuitive hypothesis made in⁶⁰, that the actual zero-field IC phase of β - Li_2IrO_3 is a long-wavelength twisting of a nearby commensurate state (the K -state). This route can be useful in analyzing related materials with analogous IC orders, such as α - Li_2IrO_3 and γ - Li_2IrO_3 ^{19,21,25–27}, and thus shed light to the delicate interplay between the various microscopic interactions, and map out the most relevant instabilities and their distinctive experimental fingerprints.

Note added after submission to preprint server – The coexistence of the zero- and finite- Q components below H^* and the connection of the large-field phase to the FM-SZ_{FM} phase of [61, 62] is consistent with a classical simulated-annealing study by Tomonari Mizoguchi and Yong Baek Kim, which was reported in a talk at the conference on *Frustrated Magnetism and Topology*, held in Kloster Nimbschen in September 2016. We thank Yong Baek Kim for bringing this to our attention. However, our interpretation for the nature of the IC component of the phase differs from the phase identified as $\overline{\text{SP}}_{a^-}$ in Refs. [61, 62], see discussion in [60].

X. Acknowledgments

We are grateful to Samuel Ducatman for collaboration on related work, and to Cristian Batista, Radu Coldea and Alexander Tsirlin for valuable discussions. This work was supported by the U.S. Department of Energy, Office of Science, Basic Energy Sciences under Award # DE-SC0018056.

¹ G. Jackeli and G. Khaliullin, “Mott Insulators in the Strong Spin-Orbit Coupling Limit: From Heisenberg to a Quantum Compass and Kitaev Models,” *Phys. Rev. Lett.* **102**, 017205 (2009).

² J. Chaloupka, George Jackeli, and Giniyat Khaliullin, “Kitaev-Heisenberg Model on a Honeycomb Lattice: Possible Exotic Phases in Iridium Oxides $A_2\text{IrO}_3$,” *Phys. Rev. Lett.* **105**, 027204 (2010).

³ Alexei Kitaev, “Anyons in an exactly solved model and beyond,” *Annals of Physics* **321**, 2 – 111 (2006).

⁴ Gang Cao and Lance DeLong, eds., *Frontiers of 4d- and 5d-Transition Metal Oxides* (World Scientific Publishing Co. Pte. Ltd., 2013).

⁵ William Witczak-Krempa, Gang Chen, Yong Baek Kim, and Leon Balents, “Correlated Quantum Phenomena in the Strong Spin-Orbit Regime,” *Ann. Rev. Cond. Matt. Phys.* **5**, 57–82 (2014).

⁶ Jeffrey G. Rau, Eric Kin-Ho Lee, and Hae-Young Kee, “Spin-Orbit Physics Giving Rise to Novel Phases in Correlated Systems: Iridates and Related Materials,” *Ann. Rev. Cond. Matt. Phys.* **7**, 195 (2016).

⁷ Simon Trebst, “Kitaev materials,” *arXiv:1701.07056* (2017).

⁸ Maria Hermanns, Itamar Kimchi, and Johannes Knolle, “Physics of the kitaev model: fractionalization, dynamical correlations, and material connections,” *arXiv:1705.01740* (2017).

⁹ Stephen M. Winter, Alexander A. Tsirlin, Maria Daghofer, Jeroen van den Brink, Yogesh Singh, Philipp Gegenwart, and Roser Valenti, “Models and materials for generalized kitaev magnetism,” *J. Phys.: Condens. Matter* **29**, 493002 (2017).

¹⁰ Saptarshi Mandal and Naveen Surendran, “Exactly solvable kitaev model in three dimensions,” *Phys. Rev. B* **79**, 024426 (2009).

¹¹ Itamar Kimchi, James G. Analytis, and Ashvin Vishwanath, “Three-dimensional quantum spin liquids in models of harmonic-

- honeycomb iridates and phase diagram in an infinite- D approximation,” *Phys. Rev. B* **90**, 205126 (2014).
- ¹² Kevin O’Brien, Maria Hermanns, and Simon Trebst, “Classification of gapless F_2 spin liquids in three-dimensional kitaev models,” *Phys. Rev. B* **93**, 085101 (2016).
- ¹³ Robert Schaffer, Subhro Bhattacharjee, and Yong Baek Kim, “Quantum phase transition in heisenberg-kitaev model,” *Phys. Rev. B* **86**, 224417 (2012).
- ¹⁴ J. Chaloupka, G. Jackeli, and G. Khaliullin, “Zigzag Magnetic Order in the Iridium Oxide Na_2IrO_3 ,” *Phys. Rev. Lett.* **110**, 097204 (2013).
- ¹⁵ Eric Kin-Ho Lee, Robert Schaffer, Subhro Bhattacharjee, and Yong Baek Kim, “Heisenberg-kitaev model on the hyperhoneycomb lattice,” *Phys. Rev. B* **89**, 045117 (2014).
- ¹⁶ Vamshi M Katukuri, S. Nishimoto, V. Yushankhai, A. Stoyanova, H. Kandpal, Sungkyun Choi, R. Coldea, I. Rousochatzakis, L. Hozoi, and Jeroen van den Brink, “Kitaev interactions between $j=1/2$ moments in honeycomb Na_2IrO_3 are large and ferromagnetic: insights from ab initio quantum chemistry calculations,” *New J. Phys.* **16**, 013056 (2014).
- ¹⁷ V. M. Katukuri, N. Satoshi, I. Rousochatzakis, H. Stoll, J. van den Brink, and L. Hozoi, “Strong magnetic frustration and anti-site disorder causing spin-glass behavior in honeycomb Li_2IrO_3 ,” *Sci Rep* (2015), 10.1038/srep14718.
- ¹⁸ Ioannis Rousochatzakis, Johannes Reuther, Ronny Thomale, Stephan Rachel, and N. B. Perkins, “Phase diagram and quantum order by disorder in the kitaev $K_1 - K_2$ honeycomb magnet,” *Phys. Rev. X* **5**, 041035 (2015).
- ¹⁹ Satoshi Nishimoto, Vamshi M. Katukuri, Viktor Yushankhai, Hermann Stoll, Ulrich K. Roessler, Liviu Hozoi, Ioannis Rousochatzakis, and Jeroen van den Brink, “Strongly frustrated triangular spin lattice emerging from triplet dimer formation in honeycomb Li_2IrO_3 ,” *Nat Commun* **7** (2016), 10.1038/ncomms10273.
- ²⁰ Yogesh Singh and P. Gegenwart, “Antiferromagnetic mott insulating state in single crystals of the honeycomb lattice material Na_2IrO_3 ,” *Phys. Rev. B* **82**, 064412 (2010).
- ²¹ Yogesh Singh, S. Manni, J. Reuther, T. Berlijn, R. Thomale, W. Ku, S. Trebst, and P. Gegenwart, “Relevance of the heisenberg-kitaev model for the honeycomb lattice iridates A_2IrO_3 ,” *Phys. Rev. Lett.* **108**, 127203 (2012).
- ²² X. Liu, T. Berlijn, W.-G. Yin, W. Ku, A. Tsvelik, Young-June Kim, H. Gretarsson, Yogesh Singh, P. Gegenwart, and J. P. Hill, “Long-range magnetic ordering in Na_2IrO_3 ,” *Phys. Rev. B* **83**, 220403 (2011).
- ²³ J. A. Sears, M. Songvilay, K. W. Plumb, J. P. Clancy, Y. Qiu, Y. Zhao, D. Parshall, and Young-June Kim, “Magnetic order in $\alpha - \text{RuCl}_3$: A honeycomb-lattice quantum magnet with strong spin-orbit coupling,” *Phys. Rev. B* **91**, 144420 (2015).
- ²⁴ R. D. Johnson, S. C. Williams, A. A. Haghighirad, J. Singleton, V. Zapf, P. Manuel, I. I. Mazin, Y. Li, H. O. Jeschke, R. Valentí, and R. Coldea, “Monoclinic crystal structure of $\alpha - \text{RuCl}_3$ and the zigzag antiferromagnetic ground state,” *Phys. Rev. B* **92**, 235119 (2015).
- ²⁵ S. C. Williams, R. D. Johnson, F. Freund, Sungkyun Choi, A. Jesche, I. Kimchi, S. Manni, A. Bombardi, P. Manuel, P. Gegenwart, and R. Coldea, “Incommensurate counterrotating magnetic order stabilized by Kitaev interactions in the layered honeycomb $\alpha - \text{Li}_2\text{IrO}_3$,” *Phys. Rev. B* **93**, 195158 (2016).
- ²⁶ A. Biffin, R. D. Johnson, I. Kimchi, R. Morris, A. Bombardi, J. G. Analytis, A. Vishwanath, and R. Coldea, “Noncoplanar and Counterrotating Incommensurate Magnetic Order Stabilized by Kitaev Interactions in $\gamma - \text{Li}_2\text{IrO}_3$,” *Phys. Rev. Lett.* **113**, 197201 (2014).
- ²⁷ KA Modic, Tess E Smidt, Itamar Kimchi, Nicholas P Breznay, Alun Biffin, Sungkyun Choi, Roger D Johnson, Radu Coldea, Pirlanda Watkins-Curry, Gregory T McCandess, *et al.*, “Realization of a three-dimensional spin-anisotropic harmonic honeycomb iridate,” *Nat. Commun.* **5** (2014), 10.1038/ncomms5203.
- ²⁸ A. Biffin, R. D. Johnson, Sungkyun Choi, F. Freund, S. Manni, A. Bombardi, P. Manuel, P. Gegenwart, and R. Coldea, “Unconventional magnetic order on the hyperhoneycomb Kitaev lattice in $\beta - \text{Li}_2\text{IrO}_3$: Full solution via magnetic resonant x-ray diffraction,” *Phys. Rev. B* **90**, 205116 (2014).
- ²⁹ T. Takayama, A. Kato, R. Dinnebier, J. Nuss, H. Kono, L. S. I. Veiga, G. Fabbris, D. Haskel, and H. Takagi, “Hyperhoneycomb iridate $\beta - \text{Li}_2\text{IrO}_3$ as a platform for kitaev magnetism,” *Phys. Rev. Lett.* **114**, 077202 (2015).
- ³⁰ S.-H. Baek, S.-H. Do, K.-Y. Choi, Y. S. Kwon, A. U. B. Wolter, S. Nishimoto, Jeroen van den Brink, and B. Büchner, “Evidence for a Field-Induced Quantum Spin Liquid in $\alpha - \text{RuCl}_3$,” *Phys. Rev. Lett.* **119**, 037201 (2017).
- ³¹ R. Yadav, N. A. Bogdanov, V. M. Katukuri, S. Nishimoto, J. van den Brink, and L. Hozoi, “Kitaev exchange and field-induced quantum spin-liquid states in honeycomb $\alpha - \text{RuCl}_3$,” *Sci Rep.* **6**, 37925 (2016).
- ³² J. A. Sears, Y. Zhao, Z. Xu, J. W. Lynn, and Young-June Kim, “Phase diagram of $\alpha - \text{RuCl}_3$ in an in-plane magnetic field,” *Phys. Rev. B* **95**, 180411 (2017).
- ³³ Jiacheng Zheng, Kejing Ran, Tianrun Li, Jinghui Wang, Pengshuai Wang, Bin Liu, Zhengxin Liu, B. Normand, Jinsheng Wen, and Weiqiang Yu, “Gapless spin excitations in the field-induced quantum spin liquid phase of $\alpha - \text{RuCl}_3$,” *arXiv:1703.08474* (2017).
- ³⁴ Richard Hentrich, Anja U. B. Wolter, Xenophon Zotos, Wolfram Brenig, Domenic Nowak, Anna Isaeva, Thomas Doert, Arnab Banerjee, Paula Lampen-Kelley, David G. Mandrus, Stephen E. Nagler, Jennifer Sears, Young-June Kim, Bernd Büchner, and Christian Hess, “Large field-induced gap of Kitaev-Heisenberg paramagnons in $\alpha - \text{RuCl}_3$,” *arXiv:1703.08623* (2017).
- ³⁵ C. Wellm, J. Zeisner, A. Alfonsov, A. U. B. Wolter, M. Roslova, A. Isaeva, T. Doert, M. Vojta, B. Büchner, and V. Kataev, “Signatures of low-energy fractionalized excitations in $\alpha - \text{RuCl}_3$ from field-dependent microwave absorption,” *arXiv:1710.00670* (2017).
- ³⁶ Alejandro Ruiz, Alex Frano, Nicholas P. Breznay, Itamar Kimchi, Toni Helm, Iain Oswald, Julia Y. Chan, R. J. Birgeneau, Z. Islam, and James G. Analytis, “Correlated states in $\beta - \text{Li}_2\text{IrO}_3$ driven by applied magnetic fields,” *Nat. Commun.* **8**, 961 (2017).
- ³⁷ M. Majumder, R.S. Manna, G. Simutis, J.C. Orain, T. Dey, F. Freund, A. Jesche, R. Khasanov, P.K. Biswas, E. Bykova, N. Dubrovinskaia, L.S. Dubrovinsky, R. Yadav, L. Hozoi, S. Nishimoto, A.A. Tsirlin, and P. Gegenwart, “Breakdown of magnetic order in the pressurized Kitaev iridate $\beta - \text{Li}_2\text{IrO}_3$,” *arXiv:1802.06819* (2018).
- ³⁸ K. A. Modic, B. J. Ramshaw, J. B. Betts, Nicholas P. Breznay, James G. Analytis, Ross D. McDonald, and Arkady Shekhter, “Robust spin correlations at high magnetic fields in the harmonic honeycomb iridates,” *Nat. Commun.* **8** (2017), 10.1038/s41467-017-00264-6.
- ³⁹ Gia-Wei Chern, Yuriy Sizyuk, Craig Price, and Natalia B. Perkins, “Kitaev-Heisenberg model in a magnetic field: Order-by-disorder and commensurate-incommensurate transitions,” *Phys. Rev. B* **95**, 144427 (2017).
- ⁴⁰ Lukas Janssen, Eric C. Andrade, and Matthias Vojta, “Honeycomb-Lattice Heisenberg-Kitaev Model in a Magnetic Field: Spin Canting, Metamagnetism, and Vortex Crystals,” *Phys. Rev. Lett.* **117**, 277202 (2016).

- ⁴¹ Lukas Janssen, Eric C. Andrade, and Matthias Vojta, “Magnetization processes of zigzag states on the honeycomb lattice: Identifying spin models for α - RuCl_3 and Na_2IrO_3 ,” *Phys. Rev. B* **96**, 064430 (2017).
- ⁴² Stephen M. Winter, Kira Riedl, David Kaib, Radu Coldea, and Roser Valentí, “Probing α - RuCl_3 beyond magnetic order: Effects of temperature and magnetic field,” *Phys. Rev. Lett.* **120**, 077203 (2018).
- ⁴³ K. Kitagawa, T. Takayama, Y. Matsumoto, A. Kato, R. Takano, Y. Kishimoto, R. Dinnebier, G. Jackeli, and H. Takagi, “Quantum liquid of kramers doublets on a honeycomb lattice,” unpublished (2018).
- ⁴⁴ Kevin Slagle, Wonjune Choi, Li Ern Chern, and Yong Baek Kim, “Theory of a quantum spin liquid in the hydrogen-intercalated honeycomb iridate $\text{h}_3\text{liir}_2\text{o}_6$,” *Phys. Rev. B* **97**, 115159 (2018).
- ⁴⁵ L. S. I. Veiga, M. Etter, K. Glazyrin, F. Sun, C. A. Escanhoela, G. Fabbri, J. R. L. Mardegan, P. S. Malavi, Y. Deng, P. P. Stavropoulos, H.-Y. Kee, W. G. Yang, M. van Veenendaal, J. S. Schilling, T. Takayama, H. Takagi, and D. Haskel, “Pressure tuning of bond-directional exchange interactions and magnetic frustration in the hyperhoneycomb iridate β - Li_2IrO_3 ,” *Phys. Rev. B* **96**, 140402 (2017).
- ⁴⁶ Nicholas P. Breznay, Alejandro Ruiz, Alex Frano, Wenli Bi, Robert J. Birgeneau, Daniel Haskel, and James G. Analytis, “Resonant x-ray scattering reveals possible disappearance of magnetic order under hydrostatic pressure in the kitaev candidate γ - Li_2IrO_3 ,” *Phys. Rev. B* **96**, 020402 (2017).
- ⁴⁷ G. Bastien, G. Garbarino, R. Yadav, F. J. Martinez-Casado, R. Beltrn Rodríguez, Q. Stahl, M. Kusch, S. P. Limandri, R. Ray, P. Lampen-Kelley, D. G. Mandrus, S. E. Nagler, M. Roslova, A. Isaeva, T. Doert, L. Hozoi, A. U. B. Wolter, B. Büchner, J. Geck, and J. van den Brink, “Pressure-induced dimerization and valence bond crystal formation in the Kitaev-Heisenberg magnet α - RuCl_3 ,” [arXiv:1802.09861](https://arxiv.org/abs/1802.09861) (2018).
- ⁴⁸ Tobias Biesner, Sananda Biswas, Weiwu Li, Yohei Saito, Andrej Pustogow, Michaela Altmeyer, Anja U. B. Wolter, Bernd Büchner, Maria Roslova, Thomas Doert, Stephen M. Winter, Roser Valentí, and Martin Dressel, “Detuning the Honeycomb of α - RuCl_3 : Pressure-Dependent Optical Studies Reveal Broken Symmetry,” [arXiv:1802.10060](https://arxiv.org/abs/1802.10060) (2018).
- ⁴⁹ Heung-Sik Kim, Yong Baek Kim, and Hae-Young Kee, “Revealing frustrated local moment model for pressurized hyperhoneycomb iridate: Paving the way toward a quantum spin liquid,” *Phys. Rev. B* **94**, 245127 (2016).
- ⁵⁰ Ravi Yadav, Stephan Rachel, Liviu Hozoi, Jeroen van den Brink, and George Jackeli, “Pressure-tuned magnetic interactions in honeycomb Kitaev materials,” [arXiv:1802.01051](https://arxiv.org/abs/1802.01051) (2018).
- ⁵¹ J. P. Clancy, H. Gretarsson, J. A. Sears, Yogesh Singh, S. Desgreniers, Kavita Mehlawat, Samar Layek, Gregory Kh. Rozenberg, Yang Ding, M. H. Upton, D. Casa, N. Chen, Junhyuck Im, Yongjae Lee, R. Yadav, L. Hozoi, D. Efremov, J. van den Brink, and Young-June Kim, “Pressure-driven collapse of the relativistic electronic ground state in a honeycomb iridate,” [arXiv:1803.04056](https://arxiv.org/abs/1803.04056) (2018).
- ⁵² V. Hermann, M. Altmeyer, J. Ebad-Allah, F. Freund, A. Jesche, A. A. Tsirlin, M. Hanfland, P. Gegenwart, I. I. Mazin, D. I. Khomskii, R. Valentí, and C. A. Kuntscher, “Competition between spin-orbit coupling, magnetism, and dimerization in the honeycomb iridates: α - Li_2IrO_3 under pressure,” *Phys. Rev. B* **97**, 020104 (2018).
- ⁵³ S. K. Choi, R. Coldea, A. N. Kolmogorov, T. Lancaster, I. I. Mazin, S. J. Blundell, P. G. Radaelli, Yogesh Singh, P. Gegenwart, K. R. Choi, S.-W. Cheong, P. J. Baker, C. Stock, and J. Taylor, “Spin Waves and Revised Crystal Structure of Honeycomb Iridate Na_2IrO_3 ,” *Phys. Rev. Lett.* **108**, 127204 (2012).
- ⁵⁴ Feng Ye, Songxue Chi, Huibo Cao, Bryan C. Chakoumakos, Jaime A. Fernandez-Baca, Radu Custelcean, T. F. Qi, O. B. Korneta, and G. Cao, “Direct evidence of a zigzag spin-chain structure in the honeycomb lattice: A neutron and x-ray diffraction investigation of single-crystal Na_2IrO_3 ,” *Phys. Rev. B* **85**, 180403 (2012).
- ⁵⁵ Sae Hwan Chun, Jong-Woo Kim, Jungho Kim, H. Zheng, Constantinos C. Stoumpos, C. D. Malliakas, J. F. Mitchell, Kavita Mehlawat, , Yogesh Singh, Y. Choi, T. Gog, A. Al-Zein, M. Moretti Sala, M. Krisch, J. Chaloupka, G. Jackeli, G. Khalullin, and B. J. Kim, “Direct evidence for dominant bond-directional interactions in a honeycomb lattice iridate Na_2IrO_3 ,” *Nat Phys* **10**, 1038 (2015).
- ⁵⁶ K. W. Plumb, J. P. Clancy, L. J. Sandilands, V. Vijay Shankar, Y. F. Hu, K. S. Burch, Hae-Young Kee, and Young-June Kim, “ α - RuCl_3 : A spin-orbit assisted Mott insulator on a honeycomb lattice,” *Phys. Rev. B* **90**, 041112 (2014).
- ⁵⁷ Yumi Kubota, Hidekazu Tanaka, Toshio Ono, Yasuo Narumi, and Koichi Kindo, “Successive magnetic phase transitions in α - RuCl_3 : XY-like frustrated magnet on the honeycomb lattice,” *Phys. Rev. B* **91**, 094422 (2015).
- ⁵⁸ M. Majumder, M. Schmidt, H. Rosner, A. A. Tsirlin, H. Yasuoka, and M. Baenitz, “Anisotropic $\text{Ru}^{3+}4d^5$ magnetism in the α - RuCl_3 honeycomb system: Susceptibility, specific heat, and zero-field NMR,” *Phys. Rev. B* **91**, 180401 (2015).
- ⁵⁹ A Banerjee, CA Bridges, J-Q Yan, AA Aczel, L Li, MB Stone, GE Granroth, MD Lumsden, Y Yiu, J Knolle, *et al.*, “Proximate Kitaev quantum spin liquid behaviour in a honeycomb magnet,” *Nature materials* (2016), 10.1038/nmat4604.
- ⁶⁰ Samuel Ducatman, Ioannis Rousochatzakis, and Natalia B. Perkins, “Magnetic structure and excitation spectrum of the hyperhoneycomb Kitaev magnet β - Li_2IrO_3 ,” *Phys. Rev. B* **97**, 125125 (2018).
- ⁶¹ Eric Kin-Ho Lee and Yong Baek Kim, “Theory of magnetic phase diagrams in hyperhoneycomb and harmonic-honeycomb iridates,” *Phys. Rev. B* **91**, 064407 (2015).
- ⁶² Eric Kin-Ho Lee, Jeffrey G. Rau, and Yong Baek Kim, “Two iridates, two models, and two approaches: A comparative study on magnetism in three-dimensional honeycomb materials,” *Phys. Rev. B* **93**, 184420 (2016).
- ⁶³ From these relations it follows, in particular, that the \hat{b} -axis is special because the Kitaev exchange on the z -type of bonds couples the spin projections along precisely this axis.³⁶
- ⁶⁴ Here and in Eq. (5) we have multiplied by a factor of $2S$ compared to the expressions given in Ref. [60].
- ⁶⁵ We should note that these *ab initio* calculations give a negative J , which on the basis of the J - K - Γ model cannot deliver the IC order reported experimentally.
- ⁶⁶ Vamshi M. Katukuri, Ravi Yadav, Liviu Hozoi, Satoshi Nishimoto, and Jeroen van den Brink, “The vicinity of hyperhoneycomb β - Li_2IrO_3 to a three-dimensional kitaev spin liquid state,” *Sci. Rep.* **6**, 29585 (2016).
- ⁶⁷ Ioannis Rousochatzakis and Natalia B. Perkins, “Classical spin liquid instability driven by off-diagonal exchange in strong spin-orbit magnets,” *Phys. Rev. Lett.* **118**, 147204 (2017).
- ⁶⁸ We know from other anisotropic models of this type (see e.g. Ref. [18]) that the spin length reduction by quantum fluctuations is otherwise very small due to the anisotropy spin gap.